Harmonically forced enclosed swirling flow

Y. D. Cui,[1] J. M. Lopez,[2,a)] T. T. Lim,[3] and F. Marques[4]
[1]*Temasek Laboratories, National University of Singapore, Singapore 119260, Singapore*
[2]*School of Mathematical and Statistical Sciences, Arizona State University, Tempe, Arizona 85287, USA*
[3]*Department of Mechanical Engineering, National University of Singapore, Singapore 119260, Singapore*
[4]*Departament de Física Aplicada, Universitat Politècnica de Catalunya, 08034 Barcelona, Spain*

(Received 24 May 2008; accepted 10 February 2009; published online 24 March 2009)

The response of steady state vortex flows in an enclosed circular cylinder driven by the harmonic modulation of the rotating end wall is investigated experimentally and numerically. Three dynamic regimes have been identified, with a continuous variation in forcing frequency between them. For very low forcing frequency, the synchronous flow approaches quasistatic adjustment, and for very large forcing frequencies the oscillations in the synchronous flow are localized in the boundary layers on the various cylinder walls. These localized wall oscillations drive the synchronous flow in the cylinder interior to the underlying axisymmetric steady basic state. The third regime occurs for forcing frequencies in the range of the most dangerous axisymmetric Hopf eigenfrequencies, with the 1:1 resonances leading to greatly enhanced oscillation amplitudes localized in the axis region where the flow manifests vortex breakdown recirculation zones. © *2009 American Institute of Physics*. [DOI: 10.1063/1.3093236]

I. INTRODUCTION

There has been much interest in the swirling flow in an enclosed cylinder driven by the rotation of an end wall for applications where a high degree of mixing is desired, such as in microbioreactors, although at a low level of shear stress.[1–5] The interest stems from the very good mixing properties when the flow is operated above the threshold for self-sustained oscillations as these provide chaotic mixing.[6] The concern is, of course, that the chaotic mixing is only present when the Reynolds number is above a critical level for the Hopf bifurcation, and so one would like to achieve comparable oscillations at lower Reynolds numbers, thereby subjecting the biological material to lower damaging stress levels.

The response of an axisymmetric time-periodic swirling flow in a confined cylinder to harmonically modulated rotation of the end wall driving the flow has been recently investigated.[7] That study considered the flow in a cylinder of height-to-radius aspect ratio $H/R=2.5$ and Reynolds number $\mathrm{Re}=2800$ (which is about 3.3% above the critical $\mathrm{Re}=2710$ for the Hopf bifurcation spawning the limit cycle flow), characterized by a large double vortex breakdown bubble undergoing large amplitude pulsations along the axis. They showed that for very small forcing amplitudes, the resultant flow is generally quasiperiodic, possessing both the natural frequency of the unforced limit cycle state together with the forcing frequency. As would be expected when harmonically forcing a limit cycle, they found resonance behavior associated with Arnold tongues when the forcing frequency and the natural (Hopf) frequency of the limit cycle were in rational ratios. For modulation amplitudes between 2% and 5% of the mean rotation of the end wall (depending irregularly on the forcing frequency), the resultant flow becomes synchronous with the forcing frequency as the natural frequency is completely suppressed. They also found that for low forcing frequencies (less than about twice the natural frequency), the forced limit cycle consists of an enhanced vortex breakdown recirculation bubble on the axis oscillating with larger amplitude than in the unforced case, whereas for larger forcing frequencies, the forced limit cycle has a (nearly) stationary vortex breakdown bubble on the axis, with the flow oscillations localized near the cylinder sidewall, and, in particular, near the junction where the rotating end wall and the stationary cylinder wall meet.

Two things emerged from that study.[7] One was quite expected, that for very low amplitude forcing the response is well described by resonant behavior. However, the second finding was not directly obvious, and it seems to be unrelated to resonances of the type described by the Arnold circle map model.[8] To help clarify the spatiotemporal responses at the slightly higher forcing amplitudes (2%–5% of the mean Re), we explore in this paper the response to the same type of harmonic forcing, but at mean Re below the critical value for the Hopf bifurcation, so that we are harmonically forcing a stable axisymmetric steady state. The response in this situation is a limit cycle flow synchronous with the imposed modulation frequency. However, there are distinct frequencies at which the amplitude of this synchronous limit cycle is quite large. One such spike clearly corresponds to the natural frequency of the nearby Hopf bifurcation. However there are other spikes in the response amplitude for quite different frequencies. One expectation is that these may be due to rational ratios between the primary Hopf frequency and the modulation frequency. However, on closer examination it becomes evident that these spikes correspond to axisymmetric limit cycles that appear in secondary Hopf bifurcations from

a)Electronic mail: lopez@math.asu.edu.

the basic state at higher Re. These secondary states and their frequencies have been previously identified from linear stability analysis,[9] and their signatures have been observed experimentally[10] and in direct numerical simulations.[11] What becomes apparent is that it is the spatiotemporal characteristics of the harmonic forcing and not just the temporal characteristics that determine the flow response. Furthermore, it is not just the limit cycle that bifurcates supercritically in the primary Hopf bifurcation that is responsible for the flow response to harmonic forcing, but that a number of limit cycles are involved. What is perhaps unexpected is that these other limit cycles do not bifurcate from the basic state until the Reynolds number is much larger than the mean Re at which the harmonic forcing is being applied, and that in the unforced system these limit cycles are never stable.

Interest in harmonically forced fluid dynamic systems is quite widespread, see the review article of Davis.[12] Other examples of periodic forcing of fluid systems include harmonically forced Taylor–Couette flows,[13–16] the transverse oscillations of a cylinder,[17,18] periodically driven cavity flow,[19–22] modulated rotating convection.[23–26] and mixing in microfluidics.[27] The problem investigated in this paper falls into this class, and has the added advantage of being generic as unlike in the other examples, symmetries play no role in the observed dynamics.

The combined experimental and numerical simulations of the Navier–Stokes equations presented here, together with the prior linear stability analysis of the unforced system, lead to a coherent flow physics picture of how the oscillatory Stokes layer on the modulated rotating disk leads to the formation of an oscillatory sidewall layer whose spatiotemporal structure resonates with the Hopf eigenfunctions of the basic state, leading to the observed flow response to harmonic forcing.

II. GOVERNING EQUATIONS AND NUMERICAL SCHEME

Consider the flow in a circular cylinder of radius R and depth H, with the bottom lid rotating at a modulated rate $\Omega[1+A\sin(\Omega_f t^*)]$, where t^* is dimensional time in seconds, Ω rad/s is the mean rotation, Ω_f rad/s is the forcing frequency, and A is the relative forcing amplitude. The system is nondimensionalized using R as the length scale, and the dynamic time $1/\Omega$ as the time scale. There are four nondimensional parameters:

$$\text{Reynolds number:} \quad \mathrm{Re} = \Omega R^2/\nu,$$

$$\text{forcing amplitude:} \quad A,$$

$$\text{forcing frequency:} \quad \omega_f = \Omega_f/\Omega,$$

$$\text{aspect ratio:} \quad H/R,$$

where ν is the kinematic viscosity. The resulting nondimensional governing equations are

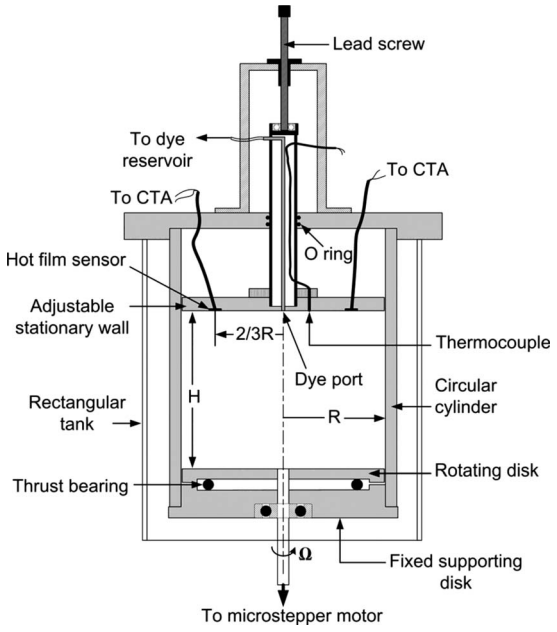

FIG. 1. Schematic of the experimental apparatus.

$$(\partial_t + \mathbf{u}\cdot\nabla)\mathbf{u} = -\nabla p + \frac{1}{\mathrm{Re}}\nabla^2\mathbf{u}, \quad \nabla\cdot\mathbf{u} = 0, \tag{1}$$

where $\mathbf{u}=(u,v,w)$ is the velocity field and p is the kinematic pressure. The boundary conditions for $\mathbf{u}$ are no slip:

$$r=1: \quad u=v=w=0, \tag{2}$$

$$z=H/R: \quad u=v=w=0, \tag{3}$$

$$z=0: \quad u=w=0, \quad v=r[1+A\sin(\omega_f t)]. \tag{4}$$

The governing equations have been solved using the second-order time-splitting method[28] combined with a pseudospectral method for the spatial discretization, utilizing a Galerkin–Fourier expansion in the azimuthal coordinate θ and Chebyshev collocation in r and z. Note that for all the results presented in this paper, the flows are axisymmetric. This has been checked by perturbing the $m=1$ Fourier coefficient and seeing that all Fourier modes decay in time to machine zero. The same code was used, and its spectral convergence tested, in an earlier study at larger Re.[7] In the present study, we have fixed $H/R=2.5$ and consider variations in Re, A and ω_f. We have used 96 spectral modes in z, 64 in r, and up to 24 in θ for nonaxisymmetric computations, and time steps $dt=2\times10^{-2}$ dynamic time units.

III. EXPERIMENTAL APPARATUS AND TECHNIQUE

The current experiments were conducted using the same apparatus as in our previous studies;[7,29] a schematic is shown in Fig. 1. It is inverted from the actual experimental setup for ease of comparison with the experimental and numerical results of others which have the rotating disk at the bottom of the cylinder (flow visualization photos are also inverted). A detailed description of the apparatus has been previously presented[7,29] and only the essential features are described here.

The apparatus consists of a Plexiglas cylinder, with a matching rotating disk at the bottom and a stationary disk at the top of the cylinder. The cylinder was fabricated from a solid piece of Plexiglas rod and was painstakingly polished to optical quality. The inner radius is $R=8.625\pm0.005$ cm and the wall thickness is 2.1 cm. The rotating disk sits neatly on a high precision thrust bearing mounted on an adjacent fixed plate, which, in turn, is push fitted into the bottom end of the cylinder to ensure accurate alignment. The edge of the rotating disk has a maximum excursion of 0.040 mm (about 0.03°) and a nominal gap of 0.40 mm between the rotating disk and the stationary cylinder. The disk was driven by a microstepper motor operating at 20 000 steps/rev, with an adjustable speed range of up to 240 rpm ($\Omega=25.1$ rad/s). The motor was controlled by software written in LABVIEW, which allows the rotation of the bottom disk to be modulated.

The working fluid was a mixture of glycerin and water (roughly 74% glycerin by weight) with kinematic viscosity $\nu=0.254\pm0.002$ cm^2/s at a room temperature of 22.3 °C. In all cases, the temperature of the mixture was monitored regularly using a thermocouple, located at the stationary end wall, to an accuracy of 0.05 °C. The viscosity was measured using a Hakke rheometer to an accuracy of about 0.8%, giving an uncertainty in the Reynolds number of about ±20 in absolute value. To minimize flow image distortion due to the curvature of the cylinder, the whole cylinder was immersed in a rectangular Plexiglas box filled with the same working fluid (both the fluid and the Plexiglas have similar refractive indices).

Due to the fact that the cylinder wall is too thick to allow efficient heat exchange between the fluid inside the cylinder and its surroundings, there is a gradual increase in the temperature of the fluid, resulting in an increase in Re at a rate $\partial\,\mathrm{Re}/\partial t\approx25/\mathrm{h}$. In the present investigation, this is not an issue as each data point required about 20 min of running time which translates into less than 0.3% change in Re. However, after each data point was taken, the experiment was halted to allow the fluid to cool down to room temperature of 22.3 °C before commencing the next experiment.

To measure the oscillatory behavior of the flow, two flush-mounting hot films (Dantec 55 R47) were attached to the surface of the stationary endplate with water-proof glue. The nominal thickness of the sensor is less 0.1 mm, and therefore its effect on the flow was negligible. These two sensors were located at 2/3 of the radius of the cylinder and 180° apart. It should be noted that the hot films were not calibrated, primarily due to the design of the glue-on hot film which makes calibration against a known flow velocity difficult; once the hot film is glued to a surface, it cannot be easily removed (without damage) for calibration in another facility. Nevertheless, calibration is not an issue for concern when measuring the temporal frequencies in a flow, and this is confirmed by the previous experimental results and detailed comparisons with numerical simulation.[7,29] Given that the frequencies of interest in the present investigation are below 1 Hz, the output signal of the hot film from the constant temperature anemometer (CTA, Dantec 55 M01) was conditioned by a low-pass filter with a cutoff frequency of 10 Hz to eliminate high frequency noise before it was amplified with an analog amplifier. The output signal was sampled at 100 Hz using a computer for subsequent analysis. To capture flow images, food dye premixed with the working solution was released very slowly into the domain through a 1.5 mm diameter hole at the center of the stationary disk, and the flow images were recorded using a CCD camera at a rate of 25 frames/s for subsequent analysis.

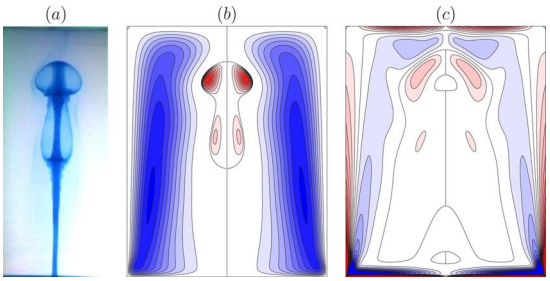

FIG. 2. (Color online) The steady axisymmetric basic state ($A=0$) at Re=2600 and $H/R=2.5$; (a) flow visualization using food dye (only the axial region is show), (b) computed streamlines ψ, and (c) computed azimuthal component of vorticity η. There are ten positive (red online) and ten negative (blue) contour levels in the ranges $\psi\in[-8.0,0.1]$ and $\eta\in[-5\times10^3,5\times10^3]$; the extreme values being darker.

In the present investigation, the Reynolds number was set at and below 2600 with A varying from 0.005 to 0.04, ω_f varying from 0.01 to 0.5, and the aspect ratio H/R was maintained at a constant value of 2.5 throughout.

IV. RESULTS AND DISCUSSIONS

A. Experiments

We begin by describing the effects of harmonic forcing on a steady vortex breakdown state at Re=2600 and $H/R=2.5$. This state is about 4% below the onset of self-sustained oscillations, which set in at Re=2710 for $H/R=2.5$ via a supercritical Hopf bifurcation with Hopf frequency $\omega_0\approx0.17$.[7] Dye flow visualization together with computed streamlines, ψ, and azimuthal vorticity, $\eta=u_z-w_r=-\psi_{rr}/r+\psi_r/r^2-\psi_{zz}/r$, of this basic state are shown in Fig. 2. The flow manifests a large steady axisymmetric vortex breakdown recirculation zone on the axis. We consider a wide range of forcing frequencies, keeping the forcing amplitude small, typically $A\lesssim0.02$. We have experimentally examined dozens of frequencies in the range $\omega_f\in[0.04,0.5]$ for various amplitudes A, and in all cases the power spectral densities (PSDs) from the time series of the hot-film outputs only have power (above the background noise level) at the forcing frequencies and its harmonics.

We first examine the effects of the modulation amplitude with a forcing frequency not in resonance with the natural frequency ω_0 (in this case, $\omega_f=0.20$, so $\omega_f/\omega_0\approx1.17$). Figure 3 presents PSD from hot-film outputs at forcing amplitudes $A=0.005$, 0.01, and 0.02. These illustrate that the resultant flow is synchronous with the imposed modulation frequency, even at very low forcing amplitudes. This is in contrast to the situation where a limit cycle flow is harmonically forced.[7] There, the resultant flow is quasiperiodic for low forcing amplitudes, and the quasiperiodic flow collapses

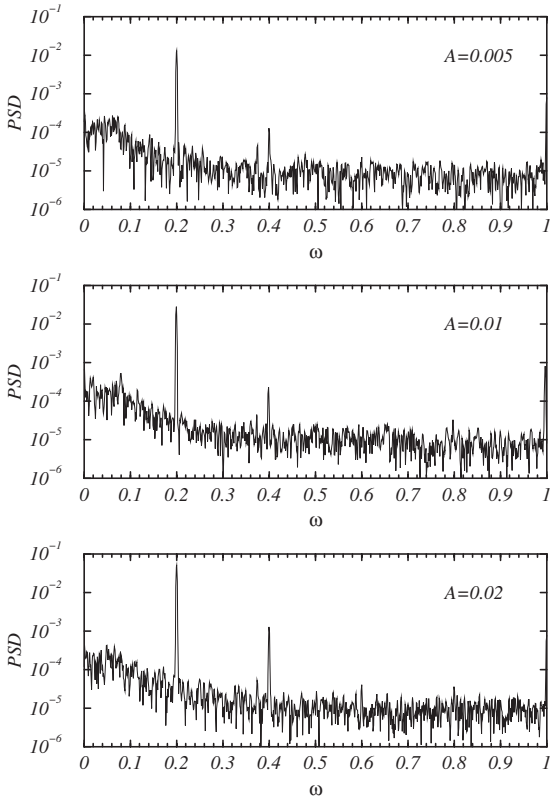

FIG. 3. Power spectral density from time series of hot-film output for flows with $H/R=2.5$, Re=2600, $\omega_f=0.2$, and forcing amplitudes A as indicated.

to a periodic flow synchronous with the forcing frequency as the forcing amplitude is increased above a critical level.

Figure 4 presents PSD from the hot-film outputs at various forcing frequencies with fixed $A=0.02$. In all the experimental runs, we checked that the hot-film outputs from the two channels are in phase (peaks matching in time), providing experimental evidence of the axisymmetric nature of the forced limit cycles. Again, the response in all cases is a flow synchronous with the forcing, but with more power when $\omega_f \approx \omega_0$.

The flow visualizations shown in Fig. 5 at $H/R=2.5$, Re=2600, $A=0.01$, and $\omega_f=0.05$, 0.171, 0.20, and 0.50 illustrate the enhanced oscillations when $\omega_f=0.171 \approx \omega_0$. In fact, at $\omega_f=0.171$, the forced synchronous flow is very similar to the natural limit cycle flow for $\mathrm{Re} > \mathrm{Re}_c \approx 2710$, exhibiting axial pulsations similar to those of the natural oscillation of

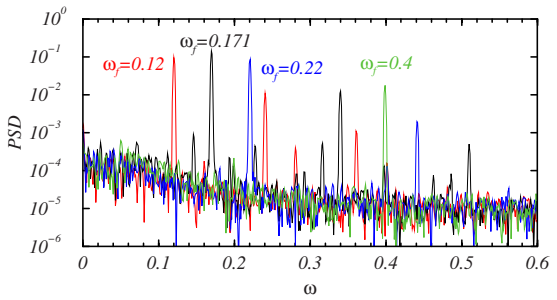

FIG. 4. (Color online) Power spectral density from time series of hot-film output for flows with $H/R=2.5$, Re=2600, $A=0.02$, and forcing frequency ω_f as indicated.

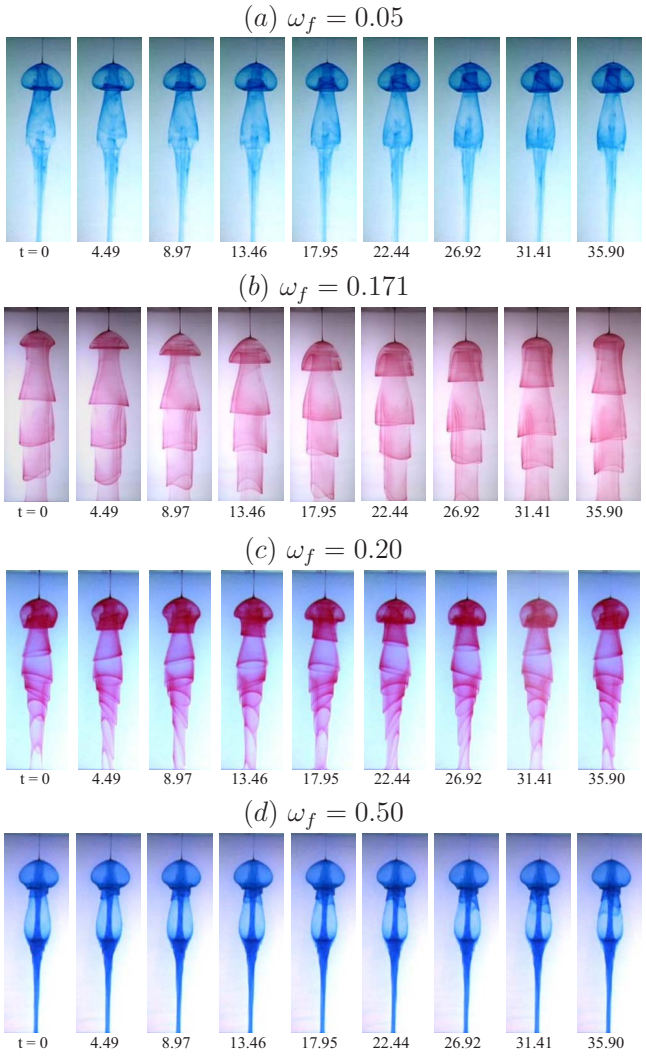

FIG. 5. (Color online) Dye flow visualization of the central vortex breakdown region at Re=2600, $H/R=2.5$, $A=0.01$, and ω_f as indicated (enhanced online). [URL: http://dx.doi.org/10.1063/1.3093236.1] [URL: http://dx.doi.org/10.1063/1.3093236.2] [URL: http://dx.doi.org/10.1063/1.3093236.3] [URL: http://dx.doi.org/10.1063/1.3093236.4]

the flow at Re=2800.[7] For $\omega_f=0.20$ the flow does not exhibit as strong oscillations, but there are still observable movements of the dye sheet, whereas for $\omega_f=0.50$ the dye sheet is quite steady and very much like that in the $A=0$ basic state shown in Fig. 2. At the very low frequency of $\omega_f=0.05$, we see that the result is a quasistatic adjustment of the flow. The movie associated with Fig. 5 shows dye visualizations over several cycles of the forced synchronous states at Re=2600, $H/R=2.5$, $A=0.01$, and $\omega_f \in [0.05, 0.50]$.

In order to obtain a more quantitative measure of the amplitude of the forced synchronous oscillations in the experiment, we present in Fig. 6 the peak-to-peak amplitude of the hot-film output at Re=2600, $H/R=2.5$ over the same range of ω_f as in the videos associated with Fig. 5, for forcing amplitudes $A=0.01$ and $A=0.02$, along with that at Re =2000 and $A=0.01$. What is most striking is that the hot-film output amplitude spikes for $\omega_f \approx \omega_0$. There are also a number of other smaller spikes, the main ones at $\omega_f \approx 0.12$ and $\omega_f \approx 0.22$. These appear to be related to the 2:3 and 4:3 reso-

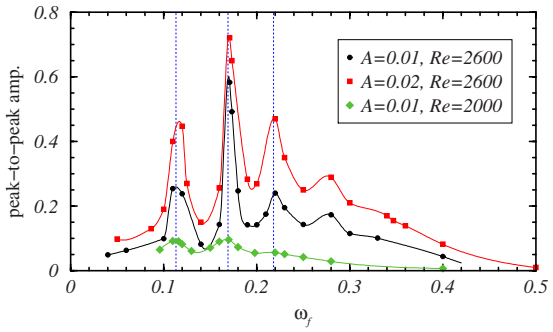

FIG. 6. (Color online) Peak-to-peak amplitudes of hot-film output with varying forcing frequency ω_f at $H/R=2.5$, Re=2600, and $A=0.01$ and 0.02. The three dotted vertical lines indicate the Hopf frequencies of the three most dangerous modes of the basic state at Re=2600, as determined in Ref. 9, where $\omega_{H1}=0.1692$, $\omega_{H2}=0.1135$, and $\omega_{H3}=0.2181$.

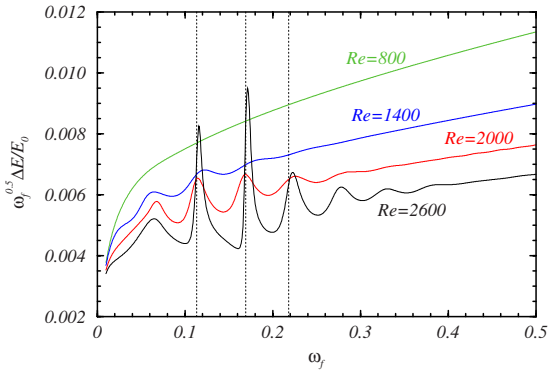

FIG. 8. (Color online) Computed variation with ω_f of the peak-to-peak amplitude of the kinetic energy relative to the kinetic energy of the basic state, $\Delta E/E_0$, and scaled by $\omega_f^{0.5}$, of the synchronous state for $A=0.01$, $H/R=2.5$, and various Re as indicated. The three dotted vertical lines indicate the Hopf frequencies of the three most dangerous modes of the basic state at Re=2600, as determined in Ref. 9, where $\omega_{H1}=0.1692$, $\omega_{H2}=0.1135$, and $\omega_{H3}=0.2181$.

nances with ω_0, but if these other spikes were simply other resonances with ω_0, one would expect the 1:2, 1:3, and 2:1 resonances to be at least comparable, but they are not evident. We conjecture that these other spikes are 1:1 resonances with secondary Hopf modes. The frequencies associated with these secondary Hopf modes were first detected experimentally in Ref. 10, computed nonlinearly in Ref. 11, but most significantly, positively correlated with secondary axisymmetric Hopf bifurcations from the basic state via linear stability analysis in Ref. 9. The results from those three studies are summarized in Fig. 7(a), showing how the frequencies of the three states vary with Re. Note that the first Hopf mode leads to a stable axisymmetric limit cycle (branch 1), while the next two Hopf modes that bifurcate from the steady basic state manifest themselves nonlinearly as a quasiperiodic nonaxisymmetric state (branch 2) and nonaxisymmetric modulated rotating waves (branch 3); in the figure only the frequency associated with the axisymmetric oscillations of the three-dimensional states is shown. The

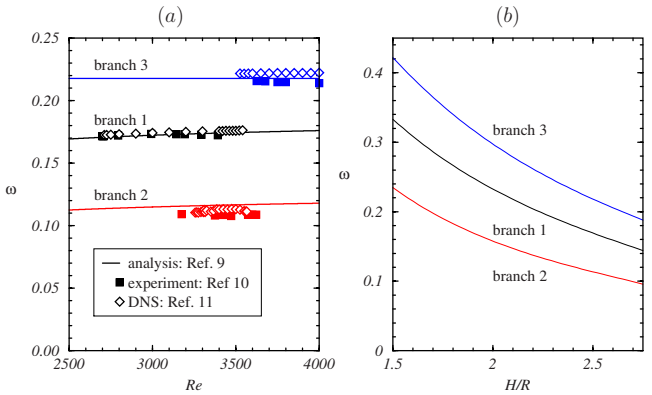

FIG. 7. (Color online) (a) Comparisons of how the frequencies of the three states vary with Re. The first Hopf mode leads to a stable axisymmetric limit cycle (branch 1), while the next two Hopf modes that bifurcate from the steady basic state manifest themselves nonlinearly as a quasiperiodic nonaxisymmetric state (branch 2) and nonaxisymmetric modulated rotating waves (branch 3); in the figure only the frequency associated with the axisymmetric oscillations of the three-dimensional states is shown. The analysis curves in the figure are the respective Hopf frequencies determined from the linear stability analysis of the basic state as a function of Re. (b) Numerically computed variation of the frequencies of the three branches with the aspect ratio H/R.

analysis curves in the figure are the respective Hopf frequencies determined from the linear stability analysis of the basic state as a function of Re. Figure 7(b) shows the variation of these frequencies with the aspect ratio H/R. The range of aspect ratios explored corresponds to the range where the first Hopf bifurcation of the base state is axisymmetric,[30] $H/R \approx (1.63, 2.76)$. There is no qualitative change, only an increase in the frequencies when decreasing the aspect ratio.

The three vertical dotted lines in Fig. 6 correspond to $\omega_f=\omega_0=0.1692$, $\omega_f=\omega_1=0.1135$, and $\omega_f=\omega_2=0.2182$, where ω_0, ω_1, and ω_2 are the Hopf frequencies of the first three Hopf modes bifurcating from the basic state. The values quoted are their values determined by linear stability analysis[9] at Re=2600. As noted earlier, the first Hopf bifurcation is at Re=2710, and the second and third occur at Re =3044 and 3122.[9] Of course, the Hopf frequencies vary with parameters (Re and H/R, as well as A and ω_f), but these variations are quite small. The good correspondence between these Hopf frequencies and the spikes in the hot-film response to ω_f lends strong experimental evidence to the spikes being 1:1 resonances with the most dangerous axisymmetric Hopf modes.

B. Numerical simulations

In the experiment, we only have quantitative measurements of the oscillation amplitudes at the location of the hot-film probes, which could give a skewed picture of the response. To get a global measure, we turn to the numerical simulations, where we are able to measure the total kinetic energy of the flow in the entire cylinder, $E(t)=0.5\int_0^{H/R}\int_0^1(u^2+v^2+w^2)rdrdz$. As a measure of the oscillation amplitude, we use the peak-to-peak amplitude of the kinetic energy, ΔE, normalized by the kinetic energy of the steady flow without modulation at the mean Re, E_0, and scaled with $\omega_f^{0.5}$. Figure 8 shows how $\omega_f^{0.5}\Delta E/E_0$ varies with ω_f for various mean Re, all with $A=0.01$. The response for Re=2600 shows the same spiky response as that observed in the hot-film data, with minor spikes at the same frequencies. At Re=2000, smaller spikes are evident at the same frequencies, and the reduction

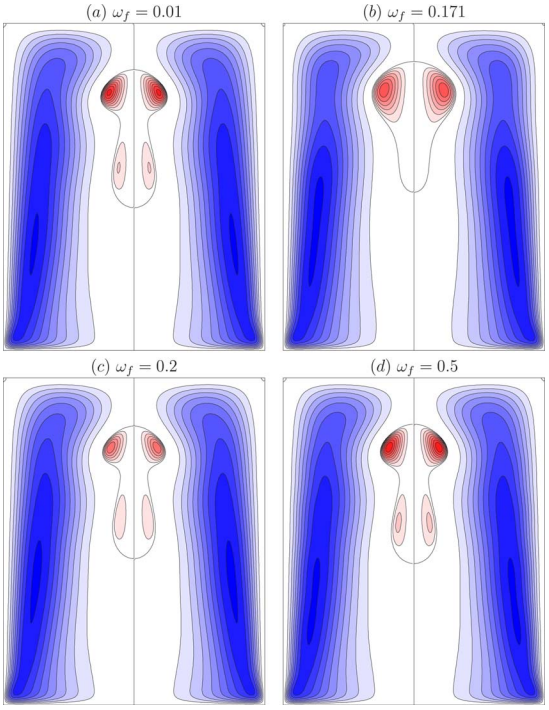

FIG. 9. (Color online) Snapshots of the stream function at various ω_f as indicated, all at Re=2600, H/R=2.5, A=0.01, and at the same phase in the forced modulation. There are ten positive (red online) and ten negative (blue) contour levels with $\psi \in [-8, 0.1]$, except of the ω_f=0.171 which has $\psi \in [-8, 0.5]$; the extreme values being darker (enhanced online). [URL: http://dx.doi.org/10.1063/1.3093236.5] [URL: http://dx.doi.org/10.1063/1.3093236.6] [URL: http://dx.doi.org/10.1063/1.3093236.7] [URL: http://dx.doi.org/10.1063/1.3093236.8]

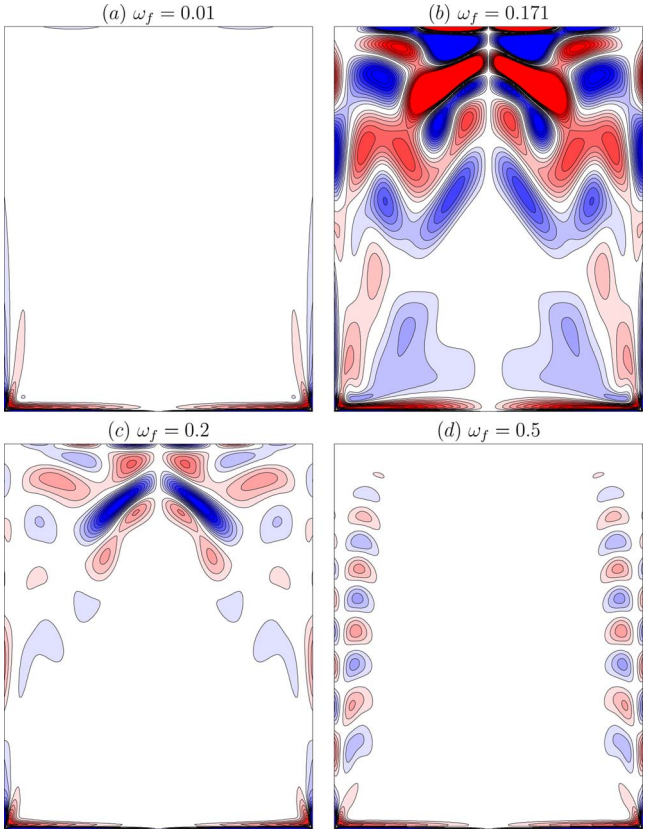

FIG. 10. (Color online) Snapshots of the azimuthal vorticity modulation, $\eta(t) - \eta_0$ (where η_0 is the steady η for A=0), at various ω_f as indicated, all at Re=2600, H/R=2.5, A=0.01, and at the same phase in the forced modulation. There are ten positive (red) and ten negative (blue) contour levels with $\eta \in [-200, 200]$; the extreme values being darker, and some clipping particularly for the ω_f=0.171 case is clearly evident (enhanced online). [URL: http://dx.doi.org/10.1063/1.3093236.9] [URL: http://dx.doi.org/10.1063/1.3093236.10] [URL: http://dx.doi.org/10.1063/1.3093236.11] [URL: http://dx.doi.org/10.1063/1.3093236.12]

in the spikes is comparable to that observed in the experiments (see Fig. 6). This all lends confidence that the local hot-film measurements are representative of the global dynamics.

A few sample solutions at Re=2600, H/R=2.5, A=0.01 at various ω_f are shown in Fig. 9, illustrating the streamlines at the start of a modulation period. The accompanying videos in the online version animate these over five periods. As was observed in the experiments, for very low ω_f=0.01, the flow undergoes a quasistatic adjustment. We have compared (not shown) the instantaneous streamlines at Re(t) with the steady streamlines of solutions with A=0 at constant Re=2600 ± 1% to arrive at this conclusion regarding the low-ω_f quasistatic adjustment. For high-ω_f, the videos show that the axial region that includes the vortex breakdown recirculation is essentially steady, with the streamlines virtually identical to those of the A=0 steady state shown in Fig. 2, and all the oscillations are concentrated in the bottom and sidewall boundary layers. The ω_f=0.2 state shows a pulsating vortex breakdown recirculation on the axis, and for ω_f=0.171 ≈ ω_0, these pulsations are significantly more pronounced, as was observed in the experiment.

While the instantaneous streamlines and the experimental dye sheets are convenient to visualize the vortex breakdown on the axis, they are not particularly enlightening in identifying the boundary layer responses to the modulations. We have found that the relative azimuthal vorticity, i.e., the difference between the instantaneous azimuthal vorticity $\eta(t)$ and the azimuthal vorticity of the steady state at A=0, η_0, is much more informative. Figure 10 shows snapshots of $\eta(t) - \eta_0$ for the same solutions as in Fig. 9, and the accompanying videos animate these over five modulation periods. These are the variations in the azimuthal vorticity distribution [see Fig. 2(c) for the mean η distribution] due to the modulations.

A number of salient features become immediately obvious. One of them is the alteration in the structure of the disk and sidewall boundary layers, particularly near the corner where the disk meets the sidewall. These alterations can be interpreted as the formation of junction vortices[31] between the stationary sidewall and the modulated rotating disk.

Another salient feature which is evident from Fig. 10 and the accompanying videos is the way that the sequence of junction vortices propagate up the sidewall and collide at the axis near the top and combine to enhance the vortex breakdown recirculation and amplify its pulsations. This is particularly dramatic at the 1:1 resonance with ω_f=0.171 ≈ ω_0. To illustrate this 1:1 resonance, we have compared $\eta(t) - \eta_0$ for Re=2600, H/R=2.5 (which without modulation corresponds to the steady vortex breakdown solution in Fig. 2) at A=0.01 and ω_f=0.171, with the natural limit cycle solution at Re=2800, H/R=2.5, and A=0. Snapshots of these two

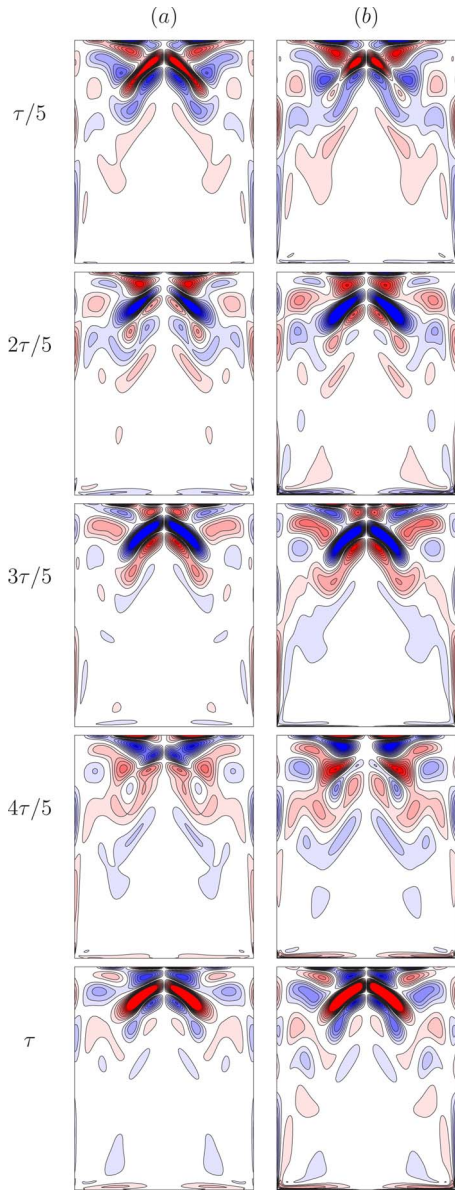

FIG. 11. (Color online) Snapshots of the azimuthal vorticity modulation, $\eta(t)-\eta_0$ (where η_0 is the steady η for $A=0$) for (a) the natural limit cycle ($A=0$) at Re=2800 and $H/R=2.5$, and (b) the synchronous state at Re =2600, $H/R=2.5$, $A=0.01$, and $\omega_f=0.171$. There are ten positive (red) and ten negative (blue) contour levels with $\eta\in[-500,500]$; the extreme values being darker (enhanced online). [URL: http://dx.doi.org/10.1063/1.3093236.13] [URL: http://dx.doi.org/10.1063/1.3093236.14]

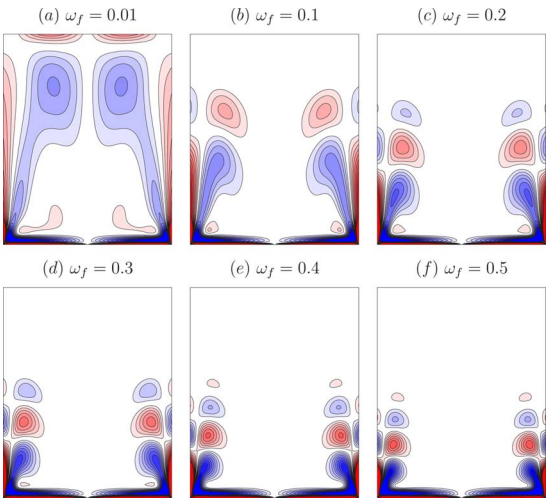

FIG. 12. (Color online) Snapshots of the azimuthal vorticity modulation, $\eta(t)-\eta_0$ (where η_0 is the steady η for $A=0$), at various ω_f as indicated, all at Re=800, $H/R=2.5$, $A=0.01$, and at the same phase in the forced modulation. There are ten positive (red) and ten negative (blue) contour levels with $\eta\in[-10,10]$; the extreme values being darker (enhanced online). [URL: http://dx.doi.org/10.1063/1.3093236.15] [URL: http://dx.doi.org/10.1063/1.3093236.16] [URL: http://dx.doi.org/10.1063/1.3093236.17] [URL: http://dx.doi.org/10.1063/1.3093236.18] [URL: http://dx.doi.org/10.1063/1.3093236.19] [URL: http://dx.doi.org/10.1063/1.3093236.20]

solutions at five phases over one period are shown in Fig. 11. Note that for the natural limit cycle at Re=2800, this Re is only about 3.3% above critical for the Hopf bifurcation, and so $\eta(t)-\eta_0$ is a very good approximation to the η-Hopf eigenfunction.[9] What is evident, particularly from the videos, is that the length scale of the junction vortex scales with ω_f^{-1} (Fig. 10), and that for $\omega_f\approx\omega_0$ the structure of the junction vortices are very similar to the vortex structure of the Hopf eigenfunction (Fig. 11). Furthermore, we have previously found[9] that the length scales of the secondary Hopf vorticity structures scale inversely with their Hopf frequencies, and hence the very good correspondence between the imposed ω_f and the length scales of the modulation-induced junction vortices leading to the other 1:1 resonance spikes in the experimental (Fig. 6) and numerical (Fig. 8) response diagrams.

These actions of the modulation-induced junction vortices at Re=2600 are complicated by the resonant interaction with the nearby Hopf modes. For lower Re, the small amplitude modulations ($A=0.01$) do not resonate with the Hopf modes (their growth rates are strongly negative), and we can view the above-described action of the disk modulation essentially in isolation of resonances with the Hopf modes. As the mean Re is reduced, the strength of the spikes (see Figs. 6 and 8) is reduced, and by mean Re=800, there is no evidence of any spiking.

At this low Re=800, we now investigate $\eta(t)-\eta_0$ over a range of ω_f at $A=0.01$. Snapshots of these are presented in Fig. 12, along with accompanying videos animating these over five periods. Now we see that the action of the modulation is to form an oscillatory modification to the layer on the modulated disk, with thickness proportional to $\mathrm{Re}^{-0.5}$; for the wide range of $\omega_f\in[0.01,0.5]$ the thickness of this modification is independent of ω_f. The reason is that the disk boundary layer is established very quickly, on the order of one disk rotation, and so a very large ω_f is needed to disrupt this. On the other hand, the development of the sidewall layer occurs on a much slower time scale. So this means that for $H/R=2.5$, $\omega_f\lesssim 0.01$ is needed to have enough time for the sidewall layer modifications to become established before the sense of the disk rotation changes and the sign of the vorticity modification in the sidewall layer is changed.

The modulation in the disk rotation leads to the formation of a sequence of junction vortices that propagate up the sidewall and whose length scale is proportional to ω_f^{-1}, the time over which they have available to develop. For small $\omega_f\lesssim 0.01$, the sidewall layer has enough time to fully de-

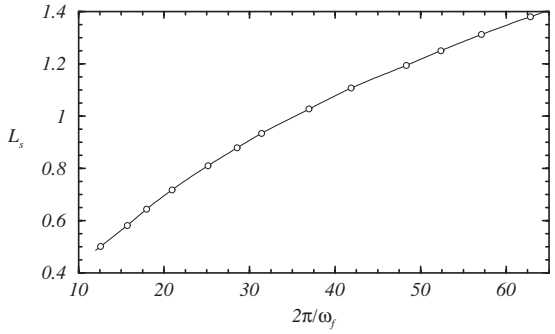

FIG. 13. Variation with modulation period $2\pi/\omega_f$ of the axial distance traveled by the junction vortex during one period, for Re=800, H/R=2.5, and A=0.01.

velop and the junction vortex completely fills the cylinder. At the other extreme, for $\omega_f > 0.3$, the sidewall layer and junction vortex only partially develop before their growth is cut off with the disk reversing its sense of rotation, resulting in a sequence of junction vortices of alternating sign traveling up the sidewall. This is particularly evident for ω_f=0.5, not only at the low Re=800 considered (Fig. 12), but also at Re =2600 (Fig. 10).

Figure 13 is a plot of the distance L_s that a junction vortex travels up the sidewall before it is cut off and a new junction vortex is generated (due to the disk acceleration/deceleration cycle), as a function of the modulation period $2\pi/\omega_f$. For the higher frequencies, the variation is linear and there is a gradual deviation from linear as ω_f is reduced. This is due to the presence of the top end wall which tends to slow the propagation of the junction vortex as it approaches the top.

C. Normal form analysis of a periodically forced Hopf bifurcation

In the experiments and the numerical simulations presented above, only solutions synchronous with the forcing have been observed below the Hopf bifurcation to periodic unsteady vortex breakdown flow. This is consistent with the classical result[32] that for sufficiently small Reynolds numbers the synchronous solution is the only stable solution. This is what we have observed in the problem under consideration, up to the Hopf bifurcation point. One may wonder if this behavior is generic and to be expected in other periodically forced Hopf bifurcations.

To address this question, we consider an analysis based on dynamical systems theory. Let us consider the normal form of a supercritical Hopf bifurcation (the primary and subsequent Hopf bifurcations from the basic state have been shown to be supercritical),[9,30] with a periodic forcing term added (for small amplitude forcing, a multiplicative forcing reduces to an additive forcing to leading order):[33]

$$\dot{\zeta} = \zeta(i - \mu - |\zeta|^2) + \epsilon e^{i\beta t}, \tag{5}$$

where time and the complex amplitude of the flow, ζ, have been conveniently scaled so that the Hopf frequency and the coefficient of $|\zeta|^2$ are equal to one. This normal form has been previously studied by Gambaudo[33] who focused on the complex dynamics following the Hopf bifurcation and in particular in the resonance horns; our earlier computational and experimental study[7] also focused on the regime following the Hopf bifurcation. Some aspects of this normal form prior to the Hopf bifurcation have also been analyzed,[17] but that study included additional parameters that complicated the dynamics and proved difficult to reconcile with the cylinder wake experiments it was intended to model. Here, we focus on the stability and response curves of the synchronous solution prior to the Hopf bifurcation. In this case $\mu > 0$; in fact μ is proportional to $(\mathrm{Re}_c - \mathrm{Re})$, where the proportionality constant may depend weakly on Re and the aspect ratio H/R. As we have scaled the time in Eq. (5) with the Hopf frequency ω_0, $\beta = \omega_f/\omega_0 = 1 + \delta$, where δ is the detuning of the forcing frequency with respect to the natural frequency, $\delta = (\omega_f - \omega_0)/\omega_0$. The amplitude of the forcing will be taken as real, because the phase can be absorbed by changing the origin of time.

We are interested in the amplitude of the synchronous response in terms of δ (detuning of the forcing frequency), ϵ (amplitude of the forcing), and μ (distance to the Hopf bifurcation point). A synchronous harmonic response is of the form $\zeta_s = ae^{i\beta t}$; substituting this into Eq. (5) results in the amplitude equation

$$a(i\delta + \mu + |a|^2) = \epsilon, \tag{6}$$

or, in terms of the modulus $|a|$,

$$|a|^2[\delta^2 + (\mu + |a|^2)^2] = \epsilon^2. \tag{7}$$

This simple algebraic equation gives implicitly the modulus of the synchronous response in terms of the parameters of the problem. As a function of δ, $|a|$ has a single maximum at $\delta = 0$, and decays to zero for $\delta \to \pm\infty$. This maximum value can be estimate as

$$\frac{|a|_{\max}}{\epsilon} \sim \epsilon^{-2/3}, \quad \text{for } \mu \ll \epsilon^{2/3}, \tag{8}$$

$$\frac{|a|_{\max}}{\epsilon} \sim \frac{1}{\mu}, \quad \text{for } \mu \gg \epsilon^{2/3}, \tag{9}$$

resulting in a large amplification rate for ϵ small, and $\mu \ll \epsilon^{2/3}$. The dependence of $|a|$ on δ, for various values of ϵ and μ, is shown in Fig. 14.

This normal form analysis shows that the synchronous solution to periodically forcing a steady state near, but below, the onset of a supercritical Hopf bifurcation has a large response that peaks at the natural Hopf frequency, and that there are no other peaks in the response curve. The amplification of the forcing can be very large for small forcing. For example, in Fig. 14(a) the amplification factor is about 4.6 for ϵ=0.1, and about 22 for ϵ=0.01.

The behavior observed in the periodically forced vortex breakdown problem is then generic below but close to a supercritical Hopf bifurcation. What is novel in the full system (considered experimentally and numerically), with respect to the two-dimensional normal form model considered in this subsection, is that there are several supercritical Hopf bifurcations in a moderate Reynolds range, and that the amplifi-

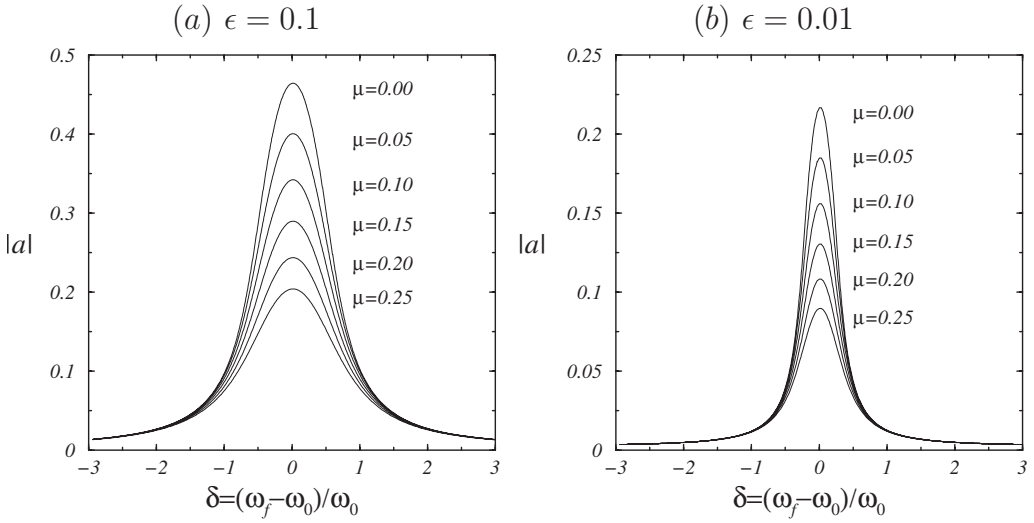

FIG. 14. Amplitude $|a|$ of the synchronous state as a function of the frequency detuning δ for forcing amplitudes (a) $\epsilon=0.1$ and (b) $\epsilon=0.01$, when the system is forced at various distances μ from the Hopf bifurcation.

cation is observed at several frequencies corresponding to the different natural Hopf frequencies of the successive Hopf bifurcations.

One may wonder if there are stable solutions below the Hopf bifurcation other than the synchronous solution given by Eq. (6). Numerical simulations of Eq. (5) suggest that the only stable solution for $\mu>0$ is the synchronous solution; this is consistent with the numerical and experimental solutions of the full system analyzed in this paper, where only synchronous solutions have been observed. However, considering that the dynamics for Re beyond the Hopf bifurcation is very complex,[7] it could be possible that additional stable solutions exist in narrow parameter regions close to the Hopf bifurcation; in the case considered here, we have not observed any additional stable solution.

In order to prove that the synchronous solution ζ_s is stable for $\mu>0$, an arbitrary perturbation is added, $\zeta=\zeta_s+\alpha$, and Eq. (5) is linearized about $\zeta=\zeta_s$ neglecting nonlinear terms in α:

$$\dot{\alpha}=\alpha(i-\mu-2|a|^2)-\zeta_s^2(t)\bar{\alpha}, \tag{10}$$

where $\bar{\alpha}$ means complex conjugate. This linear equation with periodic coefficients is solved using Floquet theory.[32] The eigenvectors of the linear problem (10) are of the form $\alpha(t)=e^{-\gamma t}f(t)$, where the eigenvalue γ is the Floquet exponent [the solution ζ_s is stable if and only if the real part of γ is positive, real $(\gamma)>0$] and f is periodic, $f(t+T)=f(t)$, where T is the forcing period $T=2\pi/\beta$. By Fourier expanding f we obtain

$$\alpha=e^{-\gamma t}\sum_{n=-\infty}^{+\infty}C_n e^{in\beta t}, \tag{11}$$

and after substitution in Eq. (10) an infinite system of equations for the coefficients C_n and γ is obtained:

$$(i(n\beta-1)-\gamma+\mu+2|a|^2)C_n=a^2\bar{C}_{2-n},\quad n\in\mathbb{Z}. \tag{12}$$

The equation for $n=1$ gives the desired information on the sign of real (γ):

$$(i\delta-\gamma+\mu+2|a|^2)C_1=a^2\bar{C}_1 \tag{13}$$

$$\Rightarrow[\mu+2|a|^2-\text{real}(\gamma)]^2+[\delta-\text{imag}(\gamma)]^2=|a|^2, \tag{14}$$

and therefore $\mu+|a|^2\le\text{real}(\gamma)\le\mu+3|a|^2$.[34] It follows that real $(\gamma)>0$ for $\mu>0$. This proves the stability of the synchronous solution below the Hopf bifurcation, and in fact, ζ_s is also stable after the Hopf bifurcation; the previous analysis shows that it is stable at least in the region where $\mu+|a|^2>0$. $|a|$ is an increasing function of ϵ for given values of μ and δ, therefore by increasing the amplitude of the forcing ϵ, the stability region of ζ_s after the Hopf bifurcation (for $\epsilon=0$) increases; this behavior was also observed in our earlier study,[7] except very close to strong resonances.

V. CONCLUSION

Using a combination of laboratory experiments, with flow visualization and hot-film anemometry, together with numerical solutions of the Navier–Stokes equations, a comprehensive investigation of the flow response to harmonic modulations of the rotation rate in an enclosed swirling flow has been undertaken. An earlier study, conducted at mean rotation rates where the flow supported self-sustained oscillations in the absence of modulations, revealed that for modulation amplitudes that were quite small (less than about 2% of the mean rotation rate), the response exhibited resonant behavior when the natural frequency and the modulation frequency were close to rational ratios. One surprising aspect of that study was the quenching of oscillations in the bulk of the flow for sufficiently large modulation frequencies. An understanding of this nonlinear behavior motivated the present study, where in order to determine the flow phys-

ics involved, we have considered mean rotation rates below the critical level for self-sustained oscillations in the unmodulated case.

Our investigation has revealed three distinct regimes in the response to harmonic modulations, characterized by the modulation frequency. For low modulation frequencies, we have a regime of quasistatic adjustment, where the swirling flow adjusts to the steady unmodulated solution at the instantaneous value of the rotation rate. In this regime, the boundary layers on the cylinder sidewall have sufficient time to fully develop during the long modulation period. At the other extreme, for high modulation frequencies, the sidewall layer does not have sufficient time to develop. As the rotating disk quickly accelerates and decelerates during the short modulation period, junction vortices form at the junction between the rotating disk and the stationary cylinder sidewall. As a junction vortex propagates up the sidewall it establishes the boundary layer. When the next junction vortex is generated, it is of opposite sense and the boundary layer development process is stopped and another layer of opposite signed vorticity is initiated. The distance up the sidewall that the junction vortex propagates and develops the sidewall layer is linearly proportional to the modulation period. The result is a sequence of junction vortices of alternating sign propagating up the sidewall. Their short wavelength and high frequency tends to inhibit the natural (Hopf) instability of the steady axisymmetric basic state, accounting for the quenching of the oscillations in the bulk observed in the earlier study. The third regime is characterized by modulation frequencies close to the Hopf frequencies of the basic state. By comparing the spatiotemporal structure of the sequence of junction vortices produced by the modulations in this range of frequencies with the vorticity eigenfunctions responsible for the self-sustained oscillations in the unmodulated problem, we have clearly identified the mechanism responsible for the large amplitude pulsations of the vortex breakdown recirculations on the axis at mean rotation rates well below critical for the self-sustained vortex breakdown oscillations.

Our prior linear stability analysis identifying the vorticity eigenstructures has been indispensable in constructing this complete picture of the resonant response to harmonic modulations. An important consequence of this study is that to achieve a strong resonant effect, it is not sufficient to only consider the temporal characteristics of the flow state, but that the imposed forcing must also match the spatial characteristics. These spatial characteristics manifest themselves in the presence of several Hopf eigenvectors bifurcating successively from the base state; and by tuning the forcing frequency, 1:1 resonances corresponding to the different spatial eigenmodes are observed. We have shown that this behavior is generic, and it may have wide-ranging implications for flow control issues in general.

ACKNOWLEDGMENTS

This work was supported by the Directorate of Research and Development, Defense Science and Technology Agency (Singapore), under the Flow Control Program No. POD-0103935, the National Science Foundation (USA) under Grant No. DMS-0505489, the Spanish Ministry of Education and Science under Grant Nos. FIS2007-61585, HA2005-0087, and AP-2004-2235, and the Catalonian Government under Grant No. SGR-00024.

[1] P. Yu, T. S. Lee, Y. Zeng, and H. T. Low, "Fluid dynamics of a microbioreactor for tissue engineering," Fluid Dyn. Mater. Process. **1**, 235 (2005).
[2] P. Yu, T. S. Lee, Y. Zeng, and H. T. Low, "Effect of vortex breakdown on mass transfer in a cell culture bioreactor," Mod. Phys. Lett. B **19**, 1543 (2005).
[3] J. Dusting, J. Sheridan, and K. Hourigan, "A fluid dynamics approach to bioreactor design for cell and tissue culture," Biotechnol. Bioeng. **94**, 1196 (2006).
[4] G. A. Thouas, J. Sheridan, and K. Hourigan, "A bioreactor model of mouse tumor progression," J. Biomed. Biotechnol. **2007**, 32754 (2007).
[5] P. Yu, T. S. Lee, Y. Zeng, and H. T. Low, "Characterization of flow behavior in an enclosed cylinder with partially rotating end wall," Phys. Fluids **19**, 057104 (2007).
[6] J. M. Lopez and A. D. Perry, "Axisymmetric vortex breakdown: Part 3. Onset of periodic flow and chaotic advection," J. Fluid Mech. **234**, 449 (1992).
[7] J. M. Lopez, Y. D. Cui, F. Marques, and T. T. Lim, "Quenching of vortex breakdown oscillations via harmonic modulation," J. Fluid Mech. **599**, 441 (2008).
[8] V. I. Arnold, "Small denominators. I. Mappings of the circumference onto itself," AMS Trans Series 2 **46**, 213 (1965) (translated from Russian).
[9] J. M. Lopez, F. Marques, and J. Sanchez, "Oscillatory modes in an enclosed swirling flow," J. Fluid Mech. **439**, 109 (2001).
[10] J. L. Stevens, J. M. Lopez, and B. J. Cantwell, "Oscillatory flow states in an enclosed cylinder with a rotating endwall," J. Fluid Mech. **389**, 101 (1999).
[11] H. M. Blackburn and J. M. Lopez, "Modulated rotating waves in an enclosed swirling flow," J. Fluid Mech. **465**, 33 (2002).
[12] S. H. Davis, "The stability of time-periodic flows," Annu. Rev. Fluid Mech. **8**, 57 (1976).
[13] A. Y. Weisberg, I. G. Kevrekidis, and A. J. Smits, "Delaying transition in Taylor–Couette flow with axial motion of the inner cylinder," J. Fluid Mech. **348**, 141 (1997).
[14] F. Marques and J. M. Lopez, "Taylor–Couette flow with axial oscillations of the inner cylinder: Floquet analysis of the basic flow," J. Fluid Mech. **348**, 153 (1997).
[15] M. Sinha, I. G. Kevrekidis, and A. J. Smits, "Experimental study of a Neimark–Sacker bifurcation in axially forced Taylor–Couette flow," J. Fluid Mech. **558**, 1 (2006).
[16] M. Avila, F. Marques, J. M. Lopez, and A. Meseguer, "Stability control and catastrophic transition in a forced Taylor-Couette system," J. Fluid Mech. **590**, 471 (2007).
[17] P. Le Gal, A. Nadim, and M. Thompson, "Hysteresis in the forced Stuart-Landau equation: Application to vortex shedding from an oscillating cylinder," J. Fluids Struct. **15**, 445 (2001).
[18] J. S. Leontini, M. C. Thompson, and K. Hourigan, "Three-dimensional transition in the wake of a transversely oscillating cylinder," J. Fluid Mech. **577**, 79 (2007).
[19] M. J. Vogel, A. H. Hirsa, and J. M. Lopez, "Spatio-temporal dynamics of a periodically driven cavity flow," J. Fluid Mech. **478**, 197 (2003).
[20] H. M. Blackburn and J. M. Lopez, "The onset of three-dimensional standing and modulated travelling waves in a periodically driven cavity flow," J. Fluid Mech. **497**, 289 (2003).
[21] F. Marques, J. M. Lopez, and H. M. Blackburn, "Bifurcations in systems with Z_2 spatio-temporal and $O(2)$ spatial symmetry," Physica D **189**, 247 (2004).
[22] J. J. F. Leung, A. H. Hirsa, H. M. Blackburn, F. Marques, and J. M. Lopez, "Three-dimensional modes in a periodically driven elongated cavity," Phys. Rev. E **71**, 026305 (2005).
[23] J. J. Niemela, M. R. Smith, and R. J. Donnelly, "Convective instability with time-varying rotation," Phys. Rev. A **44**, 8406 (1991).
[24] K. L. Thompson, K. M. S. Bajaj, and G. Ahlers, "Traveling concentric-roll patterns in Rayleigh–Bénard convection with modulated rotation," Phys. Rev. E **65**, 046218 (2002).
[25] A. Rubio, J. M. Lopez, and F. Marques, "Modulated rotating convection: Radially travelling concentric rolls," J. Fluid Mech. **608**, 357 (2008).

[26]A. Rubio, J. M. Lopez, and F. Marques, "Interacting oscillatory boundary layers and wall modes in modulated rotating convection," J. Fluid Mech. **625**, 75 (2009).
[27]D. M. Slater, C. A. López, A. H. Hirsa, and P. H. Steen, "Chaotic motions of a forced droplet-droplet oscillator," Phys. Fluids **20**, 092107 (2008).
[28]S. Hugues and A. Randriamampianina, "An improved projection scheme applied to pseudospectral methods for the incompressible Navier–Stokes equations," Int. J. Numer. Methods Fluids **28**, 501 (1998).
[29]J. M. Lopez, Y. D. Cui, and T. T. Lim, "An experimental and numerical investigation of the competition between axisymmetric time-periodic modes in an enclosed swirling flow," Phys. Fluids **18**, 104106 (2006).
[30]A. Y. Gelfgat, P. Z. Bar-Yoseph, and A. Solan, "Three-dimensional instability of axisymmetric flow in a rotating lid-cylinder enclosure," J. Fluid Mech. **438**, 363 (2001).
[31]J. J. Allen and J. M. Lopez, "Transition processes for junction vortex flow," J. Fluid Mech. **585**, 457 (2007).
[32]D. D. Joseph, *Stability of Fluid Motions I* (Springer-Verlag, New York, 1976).
[33]J. M. Gambaudo, "Perturbation of a Hopf bifurcation by an external time-periodic forcing," J. Differ. Equations **57**, 172 (1985).
[34]If $C_1=0$ a similar analysis also shows the stability of ζ_s for $\mu>0$. As the eigenvector $\alpha(t)$ is not zero, there exists a $C_n\neq 0$, and considering the equations satisfied by C_n and C_{2-n} the result $\mu+|a|^2\leq \text{real}(\gamma)\leq \mu+3|a|^2$ also follows.